BELLE2-REPORT-201X-YYY
August 11, 2016

Tau and low multiplicity physics

T. Ferber[1], K. Hayasaka[3], J. Hisano[3], E. Passemar[2]

[1] *Vancouver,* [2] *Indiana,* [3] *Nagoya*

Abstract

The report from WG8 is presented.

1 Tau and low multiplicity physics

Section author(s): H. Czyz, T. Teubner, D. Nomura, J. Hisano, E. Passemar, T. Ferber, K. Hayasaka, C. Hearty, B. Shvartz

1.1 Introduction

The enormous amount of e^+e^- collisions that are expected from the Belle II feature a unique environment for electroweak and QED studies: About 40 billion τ and μ pairs each are expected in the full dataset. The Belle II experiment will offer fantastic possibilities to study τ physics and low multiplicity final states with high precision.

In τ physics Belle II will have no competitors since the decays of τ leptons involve neutrinos which make it very difficult to study them at hadron colliders. The LHC thus has a limited τ program. τ decays offer a whole range of possible studies from a better understanding of strong interactions to precise tests of electroweak interactions including potential discovery of New Physics by a search for Lepton Flavour Violation (LFV).

Non–τ physics will profit both from the significantly larger statistics compared to Belle and BaBar, from a better detector and reconstruction software, and also from triggers especially designed to collect data for these analyses.

Five golden observables have been chosen covering τ physics, low multiplicity final states and two photon physics. They are theoretically compelling and cover both the early Belle II running and and the full Belle II dataset. They are:

- LFV: $\tau \to 3\mu$,
- Study of CP violation in $\tau \to K^0_S \pi \nu_\tau$,
- $e^+e^- \to \pi^+\pi^-$ cross section for $(g-2)_\mu$,
- Search for a Dark Photon decaying into Light Dark matter,
- Precision Measurement of the $\gamma\gamma^* \to \pi^0$ transition form factor.

All golden modes have demanding requirements for the MC event generators: The τ modes need to be implemented into TAUOLA for generation and also signal extraction, the two track modes require very high precision and the single photon search needs proper background modelling from very high rate Bhabha backgrounds.

In the following, we will explain the theoretical motivations to study these observables and we will present the sensitivity studies at Belle II.

1.2 Golden Modes

1.2.1 Lepton flavour violation in $\tau \to 3\mu$ decay

Theoretical motivations

Charged Lepton Flavor Violation (LFV) processes are very interesting to study because if they are observed, that would be a clear indication of physics beyond the Standard Model. After the observation of neutrino oscillations and if we extend the Standard Model to include the neutrino masses only, LFV can only happen through the oscillations of the neutrinos and due to GIM mechanism the prediction for the rates are at an unobservable level (e.g. $\sim 10^{-52}$ for $\mu \to e\gamma$, $\sim 10^{-45}$ for $\tau \to \mu\gamma$ [1, 2]). However, many new physics scenarios predict LFV already at an observable level with decay rates of $10^{-10} - 10^{-7}$ [3, 4, 5, 6, 7, 8, 9, 10]. While stringent bounds already exist for $\mu - e$ for instance from MEG experiment $\mathrm{Br}(\mu^+ \to e^+\gamma) < 5.7 \times 10^{-13}$ (90% CL) [11], the bounds are much weaker in the case of τ-μ or τ-e and several new physics scenarios have emerged favoring large effects for this coupling.

Moreover, the recent CMS result on Higgs LFV τ-μ coupling at the level of 1% has triggered important theoretical activities (see, e.g. []). Models that could explain such an anomaly have been presented. They all necessarily imply signals for LFV tau decays and very interesting correlations between the $H \to \mu\tau$ and tau LFV are found. **Develop!!**.

One should notice a very interesting model with Z' that explain other anomalies has been introduced. In this case $\tau \to 3\mu$ is the crucial channel to study. We have chosen $\tau \to 3\mu$ as a golden channel because it is **Develop!!**.

Experimental sensitivity studies

The results of the studies of experimental sensitivities give:

$$\mathrm{Br}(\tau \to \mu\gamma) = 4.7 \times 10^{-9}, \quad (1.1)$$

$$\mathrm{Br}(\tau \to 3\mu) = 3 \times 10^{-10}, \quad (1.2)$$

at 90% confidence level with 50 ab^{-1} at Belle II should be reached. **Develop!!**.

- Dalitz analysis (?)

1.2.2 Charged Lepton Flavor Violation in Higgs decays

The possibility of LFV in Higgs decays has been discussed some time ago [12, 13, 14]. Model-independent studies on LFV Higgs couplings have been given [15, 16, 17, 18, 19, 20, 21, 22]. Special models have been suggested to produce sizable LFV Higgs decays with observable rates at the LHC [23]. Recently, the CMS Collaboration reported a result: $\mathrm{BR}(H \to \tau\mu) < 1.57$ % (at 95% C.L.), which is translated into $\mathrm{BR}(H \to \tau\mu) = (0.89^{+0.40}_{-0.37})\%$ with 2.5 sigma significance [23].

1.2.3 Study of CP violation in $\tau \to K^0_S \pi \nu_\tau$

Theoretical motivations

Explicit studies of the decay modes $\tau^- \to K^-\pi^-\pi^+\nu_\tau$ [24, 25, 26] , $\tau^- \to \pi^- K^- K^+ \nu_\tau$ [24], have shown that sizeable CP-violating effects could be generated in some models of CP violation involving several Higgs doublets or left-right symmetry.

$\tau^- \to (3\pi)^-\nu_\tau$ [27, 28] and $\tau^- \to (4\pi)^-\nu_\tau$ [27], One should mention that BaBar has measured the $\tau^+ \to \pi^+ K_S \bar{\nu}_\tau (\geq 0\pi^0)$ [29]:

$$\begin{aligned} \mathcal{A}_\tau &= \frac{\Gamma(\tau^+ \to \pi^+ K_s \bar{\nu}_\tau) - \Gamma(\tau^- \to \pi^- K_s \bar{\nu}_\tau)}{\Gamma(\tau^+ \to \pi^+ K_s \bar{\nu}_\tau) + \Gamma(\tau^- \to \pi^- K_s \bar{\nu}_\tau)} \\ &= (-0.36 \pm 0.23 \pm 0.11)\% \,, \end{aligned} \quad (1.3)$$

2.8 σ away from the expected SM value coming from the K^0-$\bar{K}^0$ mixing: $\mathcal{A}_\tau = (0.36 \pm 0.01)\%$ [30, 31, 32]. This result could be explained by the presence of non-standard tensor interactions [33]. However, the Belle collaboration has also searched for CP violation in this decay considering $\tau^\pm$ angular distribution and has found a null result at the 0.2 - 0.3% level [34] improving the CLEO result [35] by one order of magnitude. Before drawing any firm conclusion, more precise experimental analyses are needed to clarify the compatibility between the

results from Belle and BaBar. This measurement is the Golden mode of the next Belle II experiment.

In order to be able to put constraints on new dynamics, it is very important to have the final state interactions under control. In the case of the CPV asymmetry in $\tau \to K\pi\nu_\tau$, the hadronic part is described by the scalar and vector $K\pi$ form factors that are constrained from the measurement of the $\tau \to K\pi\nu_\tau$ decay rate. Recently, to study this decay, some model-independent parametrizations for the form factors based on dispersion relations have been introduced [36, 37, 38, 39, 40, 41, 42]. They allow to take into account final state interactions. As in the case of the kaon decays [43], they would have to be used to treat correctly the hadronic part of the decays when one reaches a high-level of precision in the measurements. Moreover, in order to determine the hadronic part of these decays very accurately and to disentangle the scalar from the vector contribution, it would be very useful to measure of the forward-backward asymmetry [44]:

$$A_{FB} = \frac{d\Gamma(\cos\theta) - d\Gamma(-\cos\theta)}{d\Gamma(\cos\theta) + d\Gamma(-\cos\theta)} \; ; \qquad (1.4)$$

θ denotes the angle between the momentum of the pion and the neutrino in the hadronic rest frame. As mentioned earlier, such a measurement would also give us some insights on non-perturbative QCD and hadrodynamics for the $K\pi$ (& $K\pi$'s) system. Combining this asymmetry with the measurement of the CP violating, one would allow to disentangle the hadronic contribution from the possible new sources of CP violation. The τ forward-backward asymmetry has never been measured before.

Experimental sensitivity studies

1.2.4 $e^+e^- \to \pi^+\pi^-$ cross section for $(g-2)_\mu$ (H. Czyz, T. Teubner, D. Nomura, B. Shvartz, T. Ferber)

The discrepancy between the measurement and the Standard Model calculations for the anomalous magnetic moment of the muon $(g-2)_\mu$ is almost equal to four standard deviations. With the upcoming experiments at Fermilab [45] and J–PARC [46] we can expect factor four improvement on accuracy in each of them over the existing result [47], reducing the experimental uncertainty to about $1.6 \cdot 10^{-10}$. The current theoretical uncertainty of $4.9 \cdot 10^{-10}$ (see [48] and [49] for recent reviews) is dominated by the uncertainty coming from the two charged pion channel (see Fig. 1.1).

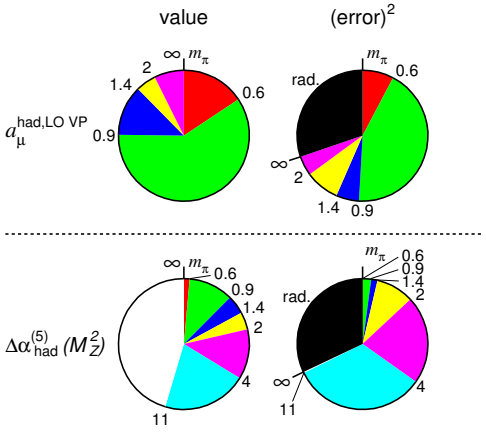

Figure 1.1: Fractions of the total contributions and errors squared, respectively, to $a_\mu^{\text{had,LO VP}}$ and $\Delta\alpha^{(5)}_{\text{had}}(M_Z^2)$, respectively, coming from various energy intervals in the dispersion integrals [**?**].)

Therefore, without significant improvement on this channel there is no hope to improve the error coming from the SM calculations. The situation here is inconclusive: The three recent most accurate experimental measurements of the cross section of the reaction $e^+e^- \to \pi^+\pi^-$ by BaBar [50], BESIII [51] and KLOE [52, 53, 54] overlap only marginally. The spread between KLOE and BaBar, not accounted in their quoted uncertainties, is bridged by BESIII results. The CMD–2 [55] and SND [56] results are not helping in sorting out this issue.

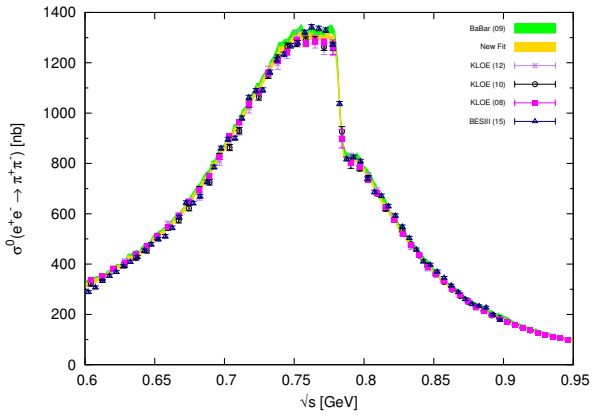

Figure 1.2: Fit with all data in the 2π channel: light (yellow) band. Radiative return data from BaBar [] are shown by the darker (green) band, whereas the KLOE [] and BESIII [] data are displayed by the markers as indicated in the plot. (Original work for B2TiP will be updated by Teubner/Nomura).

All experimental groups made a significant effort for the control of systematic errors yet the difference is not understood at all. Thus new experiment are needed. Moreover, if we like to reduce the error of $(g-2)_\mu$ significantly, the goal for the final accuracy including both statistical and systematic uncertainties should be 0.5% or lower. This is pretty challenging for both theory and experiment. (Text: Outline possible other experiments that aim at this precision: Babar updated analysis, CMD-2 updated analysis, ...)

Theory

(Text: Describe how the generator theory input is used in the analysis? Make clear that this is not the theoretical uncertainty described above for g-2. Describe why we need the muon cross section (brief explanation of the observable in the introduction before the theory subsection?) The Monte Carlo generator PHOKHARA [57], right now the generator which is the most accurate, has an accuracy of the ISR radiator function of 0.5%. This should be improved together with a technical issue of a low efficiency of the generator, when running at B factories energy with muon pair production mode. The PHOKHARA group is planning to include NNLO corrections to ISR emission in leading logarithmic approximation. This should, according to estimates, allow for lowering of the error coming from this source to the level of (0.1–0.2) %. Including the complete NNLO radiative corrections to ISR emission is more demanding and it is not planned. Another issue to be addressed is to add the missing NLO corrections to the calculation of the cross section of the reaction $e^+e^- \to \pi^+\pi^-\gamma$. The complete NLO corrections were added already to the reaction $e^+e^- \to \mu^+\mu^-\gamma$ [58], where it was found that the corrections, which were not included in PHOKHARA before, are small for all event selections used at experiments, which used the radiative return method. For $e^+e^- \to \pi^+\pi^-\gamma$ if the scalar QED is used for modelling of photon–pion interactions, one expects that the results will be similar. Yet, when including the pion form factor effects, it is difficult to predict the results and the answer will be known only after simulating the process with the complete corrections and with realistic event selections used at experiments. Works in this direction were already initiated.

Experiment

ISR photons predominately emitted at small angles and cannot be detected by the detector. In case of processes with high invariant mass of the final state, like $e^+e^- \to D(^*)\overline{D^*}$ [**?**], $e^+e^- \to D^0D^-\pi^+$ [**?**], $e^+e^- \to D_s(^*)\overline{D}_s(^*)$ [**?**] or $e^+e^- \to \Lambda_c^+\Lambda_c^-$ [**?**], a study can be performed without photon detection which led to various results in this field by the Belle experiment. These studies will be continued and extended in the Belle II experiment with much higher statistics.

However, this approach is not applicable to study of the hadronic states with an invariant mass, M^h_{inv}, below about 2 GeV like $e^+e^- \to \pi^+\pi^-$. For this study we have to use about 10 % of events with the hard photon emitted at the polar angle larger than about 30 degree. For low M^h_{inv} the hard photon energy as well as the total energy of the hadronic system is equal to about half of the

total center–of–mass (COM) energy. The pions move in the narrow cone at opposite direction to the photon with energies in the GeV range. These kinematical features are very different from multi–particle events typical for B–factories and require special study of the detection efficiency as well as track reconstruction efficiency.

A proper trigger arrangement is extremely important for ISR event studies. This was a major problem at Belle which limited precise low mass hadronic cross sections measurements. Since Bhabha scattering event rates are very high, both Belle and BaBar prescaled Bhabha triggers and vetoed low multiplicity events. To do that the Bhabha events are tagged at the level 1 trigger based on their distinct back–to–back geometry of these events and high energy deposited in the calorimeter. However, this system was not sophisticated enough at Belle and tagged many low mass ISR events as Bhabha. This resulted in a trigger efficiency of only about 60% for such low invariant mass ISR events and a strong dependence of this value from the energy threshold applied to corresponding sums of the trigger cells. Since the main goal of the Belle experiment was B–meson physics, proper attention was not paid to low multiplicity event class.

In the Belle II experiment the Bhabha tagging at the level 1 trigger will be dramatically improved using accurate trigger cell clusters determination in the trigger electronics. In the L1 trigger we will have several independent and orthogonal triggers, charged and neutral, to provide a careful measurement and data–driven monitoring of the trigger efficiency.

The BaBar experiment achieved a level of systematic accuracy in the $\pi^+\pi^-$ cross section of about 1% [50]. However, two new experiments on the muon (g-2) measurement (at FNAL [**?**] and J-PARC [**?**]) are going to reach a precision that requires at least two times better accuracy in the total hadronic cross section data in the low energy range.

The main sources of systematics at BaBar are tracking, pion and muon identification, background and ISR luminosity determination. To suppress systematic uncertainties BaBar uses the $\pi\pi/\mu\mu$ ratio for the cross section calculation. A precise measurement of the $\mu^+\mu^-$ cross section is important as well to check the consistency of the procedure in general. The measurement of this cross section was limited to about 1.5 % at Belle but will considerably improve at Belle II.

The expected performance of the tracking and particle identification at Belle II is much better than those at Belle and BaBar. We expect a large improvement of the corresponding contributions to the systematic uncertainties. High data statistics expected at Belle II experiment will provide a possibility of the careful comparison of the simulation and experimental efficiencies and determination of the corresponding corrections which should improve systematics as well. To do that we will study not only one $\pi^+\pi^-$ final state but also other ones, like $\pi^+\pi^-\pi^0$, $\pi^+\pi^-\pi^+\pi^-$, and K^+K^-.

Todo for final report: At present we do not have quantitative understanding of possible improvements of the systematic uncertainties in the hadronic cross section ISR measurements.

1.2.5 Search for a Dark Photon decaying into Light Dark matter (C. Hearty, T. Ferber)

Dark sectors are an exciting topic in particle physics. These theories introduce new particles that interact gravitationally with standard model matter, but do not interact via the electroweak or strong forces. Such particles would be dark matter that is observed astronomically.

Theory

There are a variety of such theories that involve a dark sector. One of the simplest includes a dark photon A' that mixes with strength ε to the standard model photon [59]. Annihilation

of heavy dark matter fermions would produce an A', which would decay to standard model particles, if the A' is the lightest dark sector particle. This process could explain the positron excess observed by PAMELA, LAT Fermi, and AMS [60, 61, 62]. These observations are consistent with an A' mass $M_{A'}$ in the MeV/c^2 to GeV/c^2 range. With this mass, the A' could be radiatively produced in e^+e^- collisions, $e^+e^- \to \gamma A'$.

The cross section for this process is proportional to $\varepsilon^2\alpha^2/E_{CM}^2$ [63]. The decay branching fractions of the A' are the same as a virtual photon of mass $M_{A'}$ (i.e. $e^+e^- \to \gamma^* \to X$).

A significant number of experiments have recently published results of A' searches where the A' decays into charged lepton pairs. Several other dedicated experiments will proceed over the next several years. A recent search by BaBar for the radiative production of the A' in the e^+e^- and $\mu^+\mu^-$ final states used 514 fb^{-1} of data [64]. The standard model rates for $e^+e^- \to \gamma e^+e^-$ and $e^+e^- \to \gamma\mu^+\mu^-$ are large, and the search for the A' consists of a search for a narrow peak in the dilepton mass spectrum on top of a large background.

If the A' is not the lightest dark sector particle, it will dominantly decay into light dark matter via $A' \to \chi\bar{\chi}$. Since the interaction probability of dark matter with the detector is negligible, the experimental signature of such a decay will be a mono–energetic ISR photon γ_{ISR} with energy $E_\gamma = (E_{CM}^2 - M_{A'}^2)/(2E_{CM})$. This search requires a L1 trigger that is sensitive to single photons which was not available at Belle and only partially available at BaBar. BaBar recorded about 57 fb^{-1} of data with various single photon triggers in its final year of operations, including a scan above the $\Upsilon(4S)$. 28 fb^{-1} of this data recorded at the $\Upsilon(3S)$ was used in a search for invisible decays of the light Higgs A^0, $\Upsilon(3S) \to \gamma A^0$, $A^0 \to$ invisible. The result was presented in a conference note [65], but never published.

Experiment

Monte Carlo Simulation Signal MC events ($e^+e^- \to \gamma A', A' \to \chi\bar{\chi}$) are generated using MadGraph [66] and a model based on [67] that includes a dark photon A' and fermionic dark matter χ. Each signal sample is generated using a fixed dark photon mass $m_{A'} = [0.1,\ 0.5,\ 1.0,\ 2.0,\ 3.0,\ 4.0,\ 5.0,\ 6.0,\ 7.0,\ 8.0,\ 8.5,\ 8.75,\ 9.0,\ 9.25,\ 9.5,\ 9.75]$ GeV and contains 50000 events. Events are generated for a maximal photon pseudo–rapidity of $\eta_\gamma^* < 1.681$, which corresponds to $|\cos(\theta_\gamma^*)| = 0.933$. The beam energy is set to $E^* = 10.58$ GeV. We assume a dark matter mass $m_\chi = 1$ MeV, and we set the coupling to $g_e = g_\chi$. The decay width of the dark photon is set to the tree–level width which increases slowly with $m_{A'}$ and is of $\mathcal{O}$(MeV). We assume that all decays of the A' are into $\chi\bar{\chi}$ and set the kinetic mixing parameter to $\epsilon = 1$. The resulting cross section, including vacuum polarization corrections (up to about 10 %), is shown in Fig. 1.3.

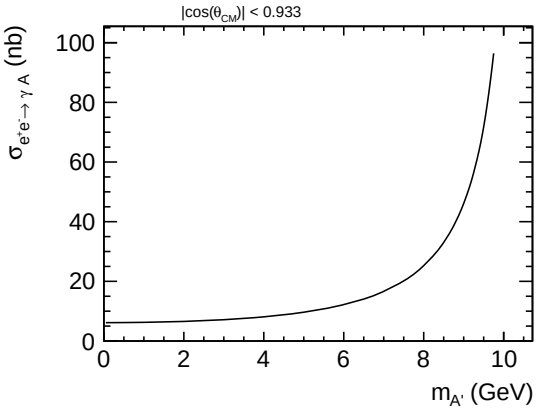

Figure 1.3: Cross section for $e^+e^- \to \gamma A'$ as function of dark photon mass $m_{A'}$ calculated using MadGraph.

The background in this analysis is dominated by high cross section QED processes $e^+e^- \to e^+e^-\gamma(\gamma)$ and $e^+e^- \to \gamma\gamma(\gamma)$ that produce one or more photons in the final states. If the charged tracks or additional photons are

not detected or out of detector acceptance, they can fake a single photon event. $e^+e^- \to \gamma\gamma(\gamma)$ events are simulated using BABAYAGA.NLO (see Sec.**??**) without any cut on the photon angles, and a minimum photon energy of 0.01 GeV which results in an effective cross section of $\sigma_{\gamma\gamma}$=25.2 nb. The phase space for radiative Bhabha events is split into three different regions: Both electrons are above $\theta^* > 1^\circ$ (A), one electron is below $\theta^* < 1^\circ$ (B) and both electrons are below $\theta^* < 1^\circ$ (C). The latter case C has a negligible cross section after event selection (see Sec.1.2.5), and is not included in the full simulation. Case A is simulated using BHWIDE [68] with a cut on the minimal electron energy of E_e >0.1 GeV. BHWIDE generates multi–photon initial state radiation, final state radiation and the interference of initial and final state radiation based on Yennie–Frautschi–Suura exponentiation (YFS) and exact NLO matrix elements. The main advantage over BABAYAGA.NLO for this particular configuration is a much higher generator speed. Some potential shortcoming of BHWIDE, like non–optimal vacuum polarization corrections and missing beam energy spread in the basf2 implementation, are negligible for this analysis. The effective cross section for the BHWIDE sample is 30,950 nb which is the by far largest contribution before further preselections (see below). The contribution for case B is simulated using three different modes of TEEGG [69]: $\mathcal{O}(\alpha^3)$ (single hard photon emission), $\mathcal{O}(\alpha^4)$ with soft corrections and $\mathcal{O}(\alpha^4)$ with hard corrections (double hard photon emission). The dominant diagram for these configurations is the t–channel amplitude and the processes are characterized by very small momentum transfers Q^2 where Z–exchange is negligible and ignored here. The $\mathcal{O}(\alpha^3)$ calculation is exact and the $\mathcal{O}(\alpha^4)$ corrections are included in the equivalent photon approximation. Additional cuts are applied for the TEEG sample: We require at least one photon with $\theta^* > 10^\circ$ and an energy of $E^* > 1.4$ GeV and no other photon above 0.1 GeV. The effective cross sections are 16.90 nb, 12.80 nb, and 4.90 nb respectively. All background samples are preselected before the events are passed to the detector simulations: We require no charged particle with p_T >0.15 GeV in $17^\circ < \theta^{lab} < 150^\circ$ and one photon with $E^{lab} > 1.4$ GeV and in $17^\circ < \theta^{lab} < 140^\circ$. We use a 0.1 fb^{-1} equivalent sample of all background samples with a reduced energy cut $E^{lab} > 0.7$ GeV and a 5.0 fb^{-1} equivalent sample for the BABAYAGA.NLO and TEEGG. The BHWIDE background has a very similar shape to the TEEGG samples and is scaled approximately according to the cross section.

The detector simulation and reconstruction use the Phase 2 BEAST 2 geometry as of release–00–07–01. All luminosity dependent beam backgrounds are scaled to 0.025 of the nominal background and all other backgrounds are scaled to 0.10 of the nominal background. Two–photon background is not included. For technical reasons the backgrounds in the PXD and SVD octant are ignored.

Trigger Efficiency The trigger efficiency has been evaluated using the L1emulator tool, which simulates the level 1 trigger response using reconstructed quantities. These studies will need to be repeated using the full trigger simulation, TSim, when it is available. We assume that the high level trigger efficiency is high.

There are two single photon triggers for physics use (i.e., not prescaled). Both look for an energy deposit in an ECL trigger tower, excluding the ring of towers closest to the beam line in each endcap. These innermost towers have very high rates of background from Bhabhas showering in CDC and VTX material outside of the detector acceptance and depositing energy in the ECL with no accompanying charged track. The angular coverage of the triggers is $18.5^\circ < \theta < 139.2^\circ$. Prescaled versions will cover the full angular range of the ECL, $12^\circ < \theta < 157^\circ$.

The first trigger requires an energy deposition $E^* > 2$ GeV, where E^* is the center of mass (COM) energy. The event must not satisfy the Bhabha or $e^+e^- \to \gamma\gamma$ vetoes. An event is labeled a Bhabha if the highest momentum track has $p^* > 3$ GeV/c, second highest has $p^* > 1$ GeV/c, they are separated by at least 143° in the COM frame, and at

least one of the two is associated with an ECL cluster with $E^* > 3\,\text{GeV}$. An event is labeled a $\gamma\gamma$ event if the two most energetic ECL clusters have $E^* > 2\,\text{GeV}$ and are separated by at least 150° in the COM frame, and the event contains no tracks with transverse momentum above $300\,\text{MeV}/c$ in the laboratory frame. Note that this is not just a single photon trigger. No requirement is placed on the number of charged tracks or additional clusters in the event, so that the trigger will be efficiency for initial state radiation production of $\pi^+\pi^-$ and similar final states. The effective cross section is estimated to be 4 nb, dominated by radiative Bhabha events.

The second trigger has a lower threshold, $E^* > 1\,\text{GeV}$, and requires that the second cluster in the event be less than 0.2 GeV. There are no other vetoes applied. The cross section is estimated to be 2.5 nb, largely due to radiative Bhabha events in which there truly is only a single photon in the acceptance of the detector.

The efficiency for signal MC as a function of A' mass, combining the two triggers, is shown in Fig. 1.4. The loss of efficiency is primarily due to detector acceptance. Trigger efficiency for high energy photons within the angular region $18.5° < \theta < 139.2°$ is 95%.

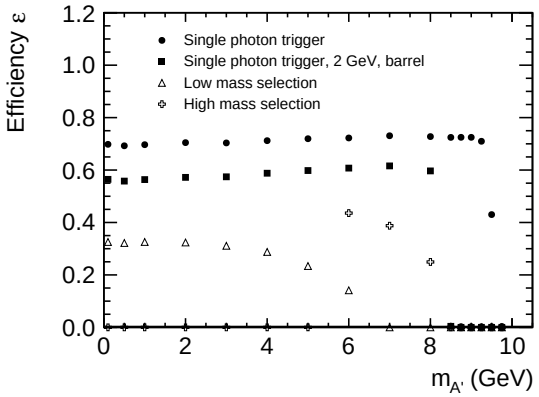

Figure 1.4: Trigger efficiency for signal MC as a function of A' mass (filled circles). The filled squares show the efficiency if the acceptance is reduced to the ECL barrel, $E^* > 2\,\text{GeV}$, a selection more relevant for the subsequent event selection. The open symbols show the overall analysis efficiency for the low mass and high mass selections discussed in Sec. 1.2.5.

Event Selection The basic event selection requires a calorimeter (ECL) cluster with center of mass energy $E^* > 1.8$ GeV, no other ECL clusters with $E^* > 0.1$ GeV, and no tracks with transverse momentum greater than 0.2 GeV/c in the center of mass frame. The cuts on the second cluster and track momentum have not been optimized, but the results shown here are not sensitive to the specific values. These criteria have high efficiency for signal; the remaining criteria are designed to suppress physics backgrounds.

Backgrounds fall into two general categories. Irreducible backgrounds are those in which the final state includes one photon and no other particles in the acceptance of the detector, which for this purpose we consider to be the full coverage of the ECL, $12° < \theta < 157°$. (In practise, efficient photon reconstruction is only available in the acceptance of the CDC, $17° < \theta < 150°$).

Simulation predicts approximately two million events of this type in 20 fb^{-1} with $E^* > 1.8$ GeV and $22° < \theta < 139°$, 85% due to radiative Bhabhas, and the remainder due to $e^+e^- \to \gamma\gamma\gamma(\gamma)$. Radiative muon pairs and other QED processes are small compared to these two sources. The kinematics of requiring all other particles be outside of the detector acceptances produces a strong correlation between the maximum COM energy of the photon and θ (Fig. 1.5).

The dominant background at higher energies are those in which there is a second photon within the detector fiducial volume that is not detected. The event may also contain a third (or more) photon outside of the acceptance. Photon detection inefficiency in the ECL is due to the following, in order of importance:

1. gap between the ECL barrel and the backwards endcap;

2. gap between the ECL barrel and the forward endcap;

3. 200 μm gaps between endcap crystals that are projective to the interaction point, plus 16 larger gaps for mechanical structure;

4. a 1–1.5 mm gap for mechanical structure in the barrel at $\theta = 90°$;

5. photons not converting in the crystal, which occurs with a probability of 3×10^{-6}.

Note that the gaps between crystals in the barrel do not project to the beam spot in either theta or phi.

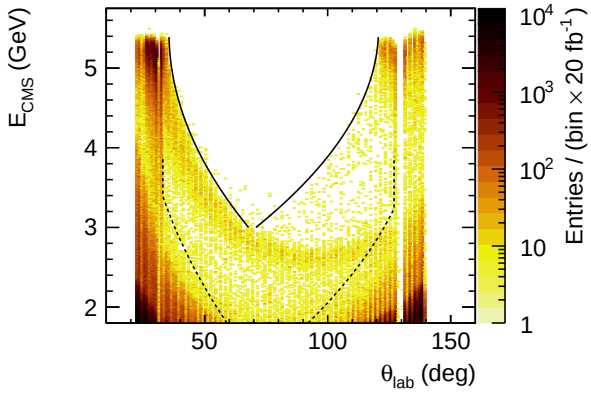

Figure 1.5: COM Energy E^* versus θ for background events satisfying all selection criteria other than the final cut on θ. The large population of events at low energies and wide angles is due to irreducible background processes. The beam-energy events near θ of 30° and 130° are due to $e^+e^- \to \gamma\gamma$ where a photon goes undetected in a gap between the ECL barrel and an endcap. The band at intermediate energies (e.g. 2.6 GeV at $\theta = 90°$ arises from three photon final states in which a near-beam-energy photon is undetected in the backward barrel–endcap gap and a second (radiative) photon is near $\theta^* = 0$. The solid lines mark the fiducial region for $m_{A'} \leq 6\,\mathrm{GeV}/c^2$; the dashed lines are for higher masses.

The KLM can also be used to detect photons. Studies with signal MC indicate that almost all KLM clusters in such events are within 25° (3D, COM) of the signal photon. To suppress backgrounds due to ECL photon inefficiency, we require that there be no KLM clusters outside of this 25° cone. At the background levels expected for Phase 2 running, 3.6% of signal MC fail this selection.

The KLM also has regions of inefficiency, primarily at the transitions from the barrel to the endcaps, at the location of the solenoid cryogenics chimney (located near the barrel / backwards endcap transition), between octants in the barrel KLM, and between sectors of the endcap KLM. The chimney and the backward transition overlap with the backwards gap in the ECL, and produce the majority of the non-irreducible backgrounds.

The kinematic distribution of background events passing the basic selection plus the additional KLM requirement is shown in Fig. 1.5. Note that we have not yet used azimuthal information. Since KLM inefficiency is concentrated at specific values of ϕ, including this information—for example, as part of a neural net or BDT—will improve the final analysis.

The final step of the selection is an energy dependent cut on θ, which rejects the vast majority of events in Fig. 1.5. Due to the limited background MC statistics in some regions of this 2D histogram, a fully automatic process was not used to select the cuts, but rather a combination of an optimization with manual intervention. For dark photon masses $m_{A'} \leq 6\,\mathrm{GeV}/c^2$ (roughly $E^* > 3$ GeV), the θ selection produces a low background region, marked with the solid lines in Fig. 1.5. This region is selected to reject the band in Fig. 1.5 corresponding to a three photon final state, where one photon is lost in the backwards ECL gap, and another is at $\theta^* = 0$. Simulation predicts 300 events per 20 fb^{-1} with $E^* > 3$ GeV between the solid lines, all due to $e^+e^- \to \gamma\gamma\gamma(\gamma)$.

At higher masses $6 < m_{A'} \leq 8\,\mathrm{GeV}/c^2$ (lower photon energy), a much wider θ region is used. It is chosen to almost completely reject the irreducible background, and to avoid the ECL endcaps, which have significantly higher inefficiency. Simulation predicts that 25,000 background events within this

theta region with $1.8 < E^* < 3.9\,\text{GeV}$, almost all due to $e^+e^- \to \gamma\gamma\gamma(\gamma)$.

Figure 1.6 shows the resulting background recoil mass distribution for the higher A' mass region, along with an example of a signal distribution.

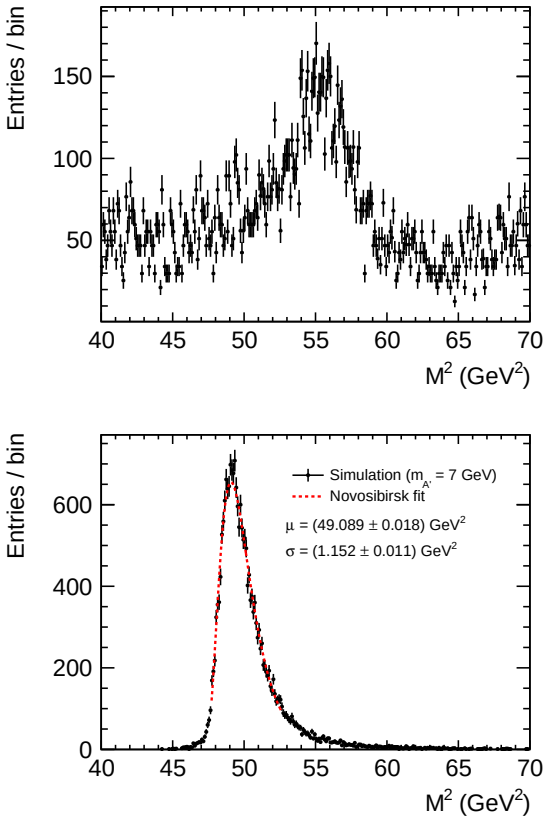

Figure 1.6: (a) Recoil mass distribution squared for background events satisfying the selection criteria for the high A' mass region. (b) Distribution for a 7 GeV/c^2 A', fit with a Novosibirsk function.

Signal Extraction The final analysis will fit the measured recoil mass squared distribution with a Novosibirsk function of appropriate width to measure the A' signal and an as-yet unspecified function for the background. The kinematic features present in the background distribution will make this quite challenging in the high mass region, and a simpler process—not suitable for the final analysis, since it uses MC truth information—has been used for this study. The procedure uses the photon energy distribution, rather than the equivalent recoil mass. The expected upper limit has been obtained for A' masses for which we have signal MC, up to an including $8\,\text{GeV}/c^2$.

For each mass the reconstructed photon COM energy has been fitted with a Novosibirsk function. The signal region is taken to be the photon energy range $[\mu_E - 3\sigma_E, \mu_E + 1.5\sigma_E]$, where μ_E and σ_E are the Novosibirsk fit parameters for that mass. This range contains between 83% and 88% of the signal.

For each mass, we obtain the expected 90% CL upper limit on the observed number of signal events μ_S from the expected number of background events μ_B. μ_B is the number of events in the signal region predicted by the generated background MC samples, scaled to $20\,\text{fb}^{-1}$. We assume that N, the number of events observed, is the integer closest to μ_B. μ_S is selected such that the Poisson probability of observing $\leq N$ events when expecting $\mu_B + \mu_S$ events is 0.1.

The upper limit on the cross section for $e^+e^- \to \gamma A'$, $A' \to$ invisible is $\sigma = \mu_S/\epsilon_S\mathcal{L}$, where ϵ_S is the signal efficiency (Fig. 1.4) and $\mathcal{L} = 20\,\text{fb}^{-1}$ is the integrated luminosity. The equivalent limit on ε is the square root of this cross section divided by the cross section calculated for $\varepsilon = 1$ (Fig. 1.3). Projected upper limits on ε are summarized as a function of A' mass in Fig. 1.7. The results are projected to be significantly better than BaBar due to the better hermiticity of the calorimeter and the efficiency of the KLM.

Systematic Uncertainties We expect that the systematic uncertainties will be dominated by uncertainties on the predicted number and kinematic properties of background events. At low A' masses, we need to quantify the residual beam-energy photon backgrounds from $e^+e^- \to \gamma\gamma$. This will require photon control samples, such as kinematically fit radiative muon pairs, or $e^+e^- \to \gamma\gamma$ events in which one photon is reconstructed at full energy and the other has low energy, corresponding to a late conversion in the ECL crystal. The backgrounds for high A' masses are dominated by events

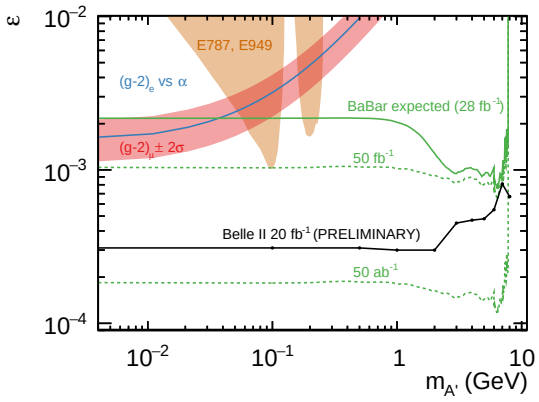

Figure 1.7: Projected upper limits on ε for the process $e^+e^- \to \gamma A'$, $A' \to$ invisible, for a $20\,\mathrm{fb}^{-1}$ Belle II data set (solid black curve). The BaBar limit is a projection based on preliminary search for invisible decays of a light Higgs []. The dashed green lines are earlier projections derived from the BaBar limit.

with one photon in the backwards barrel/endcap gap and a second near $\theta^* = 0$. The kinematically fit muon pair sample will be used to map the photon efficiency across this gap. .

1.3 Conclusions

Bibliography

[1] T.-P. Cheng and L.-F. Li, *Muon Number Nonconservation Effects in a Gauge Theory with V A Currents and Heavy Neutral Leptons*, Phys. Rev. **D16** (1977) 1425.

[2] B. W. Lee and R. E. Shrock, *Natural Suppression of Symmetry Violation in Gauge Theories: Muon - Lepton and Electron Lepton Number Nonconservation*, Phys. Rev. **D16** (1977) 1444.

[3] J. R. Ellis, M. E. Gomez, G. K. Leontaris, S. Lola, and D. V. Nanopoulos, *Charged lepton flavor violation in the light of the Super-Kamiokande data*, Eur. Phys. J. **C14** (2000) 319–334, arXiv:hep-ph/9911459 [hep-ph].

[4] J. R. Ellis, J. Hisano, M. Raidal, and Y. Shimizu, *A New parametrization of the seesaw mechanism and applications in supersymmetric models*, Phys. Rev. **D66** (2002) 115013, arXiv:hep-ph/0206110 [hep-ph].

[5] A. Dedes, J. R. Ellis, and M. Raidal, *Higgs mediated $B^0_{s,d} \to \mu\tau$, $e\tau$ and $\tau \to 3\mu$, $e\mu\mu$ decays in supersymmetric seesaw models*, Phys. Lett. **B549** (2002) 159–169, arXiv:hep-ph/0209207 [hep-ph].

[6] A. Brignole and A. Rossi, *Lepton flavor violating decays of supersymmetric Higgs bosons*, Phys. Lett. **B566** (2003) 217–225, arXiv:hep-ph/0304081 [hep-ph].

[7] G. Cvetic, C. Dib, C. S. Kim, and J. D. Kim, *On lepton flavor violation in tau decays*, Phys. Rev. **D66** (2002) 034008, arXiv:hep-ph/0202212 [hep-ph]. [Erratum: Phys. Rev.D68,059901(2003)].

[8] C.-x. Yue, Y.-m. Zhang, and L.-j. Liu, *Nonuniversal gauge bosons Z-prime and lepton flavor violation tau decays*, Phys. Lett. **B547** (2002) 252–256, arXiv:hep-ph/0209291 [hep-ph].

[9] A. Masiero, S. K. Vempati, and O. Vives, *Seesaw and lepton flavor violation in SUSY SO(10)*, Nucl. Phys. **B649** (2003) 189–204, arXiv:hep-ph/0209303 [hep-ph].

[10] T. Fukuyama, T. Kikuchi, and N. Okada, *Lepton flavor violating processes and muon g-2 in minimal supersymmetric SO(10) model*, Phys. Rev. **D68** (2003) 033012, arXiv:hep-ph/0304190 [hep-ph].

[11] J. Adam et al., MEG, *New constraint on the existence of the $\mu^+ \to e^+\gamma$ decay*, Phys. Rev. Lett. **110** (2013) 201801, arXiv:1303.0754 [hep-ex].

[12] T. P. Cheng and M. Sher, *Mass Matrix Ansatz and Flavor Nonconservation in Models with Multiple Higgs Doublets*, Phys. Rev. **D35** (1987) 3484.

[13] A. Pilaftsis, *Lepton flavor nonconservation in H0 decays*, Phys. Lett. **B285** (1992) 68–74.

[14] J. L. Diaz-Cruz and J. J. Toscano, *Lepton flavor violating decays of Higgs bosons beyond the standard model*, Phys. Rev. **D62** (2000) 116005, arXiv:hep-ph/9910233 [hep-ph].

[15] T. Han and D. Marfatia, *h —¿ mu tau at hadron colliders*, Phys. Rev. Lett. **86** (2001) 1442–1445, arXiv:hep-ph/0008141 [hep-ph].

[16] A. Goudelis, O. Lebedev, and J.-h. Park, *Higgs-induced lepton flavor violation*, Phys. Lett. **B707** (2012) 369–374, arXiv:1111.1715 [hep-ph].

[17] G. Blankenburg, J. Ellis, and G. Isidori, *Flavour-Changing Decays of a 125 GeV Higgs-like Particle*, Phys. Lett. **B712** (2012) 386–390, arXiv:1202.5704 [hep-ph].

[18] R. Harnik, J. Kopp, and J. Zupan, *Flavor Violating Higgs Decays*, JHEP **03** (2013) 026, arXiv:1209.1397 [hep-ph].

[19] S. Davidson and P. Verdier, *LHC sensitivity to the decay $h \to \tau^{\pm} mu^{\mp}$*, Phys. Rev. **D86** (2012) 111701, arXiv:1211.1248 [hep-ph].

[20] A. Falkowski, D. M. Straub, and A. Vicente, *Vector-like leptons: Higgs decays and collider phenomenology*, JHEP **05** (2014) 092, arXiv:1312.5329 [hep-ph].

[21] A. Celis, V. Cirigliano, and E. Passemar, *Lepton flavor violation in the Higgs sector and the role of hadronic τ-lepton decays*, Phys. Rev. **D89** (2014) 013008, arXiv:1309.3564 [hep-ph].

[22] A. Celis, V. Cirigliano, and E. Passemar, *Model-discriminating power of lepton flavor violating τ decays*, Phys. Rev. **D89** (2014) no. 9, 095014, arXiv:1403.5781 [hep-ph].

[23] V. Khachatryan et al., CMS, *Search for Lepton-Flavour-Violating Decays of the Higgs Boson*, Phys. Lett. **B749** (2015) 337–362, arXiv:1502.07400 [hep-ex].

[24] U. Kilian, J. G. Korner, K. Schilcher, and Y. L. Wu, *Lepton hadron angular correlations in semileptonic tau decays*, Z. Phys. **C62** (1994) 413–419.

[25] N. Mileo, K. Kiers, and A. Szynkman, *Probing sensitivity to charged scalars through partial differential widths: $\tau \to K\pi\pi\nu_\tau$ decays*, Phys. Rev. **D91** (2015) no. 7, 073006, arXiv:1410.1909 [hep-ph].

[26] K. Kiers, K. Little, A. Datta, D. London, M. Nagashima, and A. Szynkman, *CP violation in tau —¿ K pi pi nu(tau)*, Phys. Rev. **D78** (2008) 113008, arXiv:0808.1707 [hep-ph].

[27] A. Datta, K. Kiers, D. London, P. J. O'Donnell, and A. Szynkman, *CP Violation in Hadronic tau Decays*, Phys. Rev. **D75** (2007) 074007, arXiv:hep-ph/0610162 [hep-ph]. [Erratum: Phys. Rev.D76,079902(2007)].

[28] S. Y. Choi, K. Hagiwara, and M. Tanabashi, *CP violation in tau —¿ 3 pi tau-neutrino*, Phys. Rev. **D52** (1995) 1614–1626, arXiv:hep-ph/9412203 [hep-ph].

[29] J. P. Lees et al., BaBar, *Search for CP Violation in the Decay $\tau^- -> \pi^- K^0_S (>= 0\pi^0) \nu_t au$*, Phys. Rev. **D85** (2012) 031102, arXiv:1109.1527 [hep-ex]. [Erratum: Phys. Rev.D85,099904(2012)].

[30] I. I. Bigi and A. I. Sanda, *A 'Known' CP asymmetry in tau decays*, Phys. Lett. **B625** (2005) 47–52, arXiv:hep-ph/0506037 [hep-ph].

[31] G. Calderon, D. Delepine, and G. L. Castro, *Is there a paradox in CP asymmetries of tau+- —¿ K(L,S)pi+- nu decays?*, Phys. Rev. **D75** (2007) 076001, arXiv:hep-ph/0702282 [HEP-PH].

[32] Y. Grossman and Y. Nir, *CP Violation in $\tau- > \nu\pi K_S and D- > \pi K_S$: The Importance of $K_S - K_L$ Interference*, JHEP **04** (2012) 002, arXiv:1110.3790 [hep-ph].

[33] H. Z. Devi, L. Dhargyal, and N. Sinha, *Can the observed CP asymmetry in $\tau \to K\pi\nu_\tau$ be due to nonstandard tensor interactions?*, Phys. Rev. **D90** (2014) no. 1, 013016, arXiv:1308.4383 [hep-ph].

[34] M. Bischofberger et al., Belle, *Search for CP violation in $\tau \to K^0_S\pi\nu_\tau$ decays at Belle*, Phys. Rev. Lett. **107** (2011) 131801, arXiv:1101.0349 [hep-ex].

[35] G. Bonvicini et al., CLEO, *Search for CP violation in tau —¿ K pi tau-neutrino decays*, Phys. Rev. Lett. **88** (2002) 111803, arXiv:hep-ex/0111095 [hep-ex].

[36] M. Jamin, A. Pich, and J. Portoles, *Spectral distribution for the decay tau —¿ nu(tau) K pi*, Phys. Lett. **B640** (2006) 176–181, arXiv:hep-ph/0605096 [hep-ph].

[37] B. Moussallam, *Analyticity constraints on the strangeness changing vector current and applications to tau —¿ K pi nu(tau), tau —¿ K pi pi nu(tau)*, Eur. Phys. J. **C53** (2008) 401–412, arXiv:0710.0548 [hep-ph].

[38] M. Jamin, A. Pich, and J. Portoles, *What can be learned from the Belle spectrum for the decay - tau- —¿ nu(tau) K(S) pi-*, Phys. Lett. **B664** (2008) 78–83, arXiv:0803.1786 [hep-ph].

[39] D. R. Boito, R. Escribano, and M. Jamin, *K π vector form factor constrained by $\tau- > K\, pi\nu_\tau$ and K_{l3} decays*, JHEP **09** (2010) 031, arXiv:1007.1858 [hep-ph].

[40] V. Bernard, D. R. Boito, and E. Passemar, *Dispersive representation of the scalar and vector Kpi form factors for $\tau - - > K\pi nu_\tau$ and $K_{\ell 3}$ decays*, Nucl. Phys. Proc. Suppl. **218** (2011) 140–145, arXiv:1103.4855 [hep-ph].

[41] M. Antonelli, V. Cirigliano, A. Lusiani, and E. Passemar, *Predicting the τ strange branching ratios and implications for V_{us}*, JHEP **10** (2013) 070, arXiv:1304.8134 [hep-ph].

[42] V. Bernard, *First determination of $f_+(0)|V_{us}|$ from a combined analysis of $\tau \to K\pi\nu_\tau$ decay and πK scattering with constraints from $K_{\ell 3}$ decays*, JHEP **06** (2014) 082, arXiv:1311.2569 [hep-ph].

[43] M. Antonelli et al., FlaviaNet Working Group on Kaon Decays, *An Evaluation of $|V_{us}|$ and precise tests of the Standard Model from world data on leptonic and semileptonic kaon decays*, Eur. Phys. J. **C69** (2010) 399–424, arXiv:1005.2323 [hep-ph].

[44] L. Beldjoudi and T. N. Truong, *tau —¿ pi K neutrino decay and pi K scattering*, Phys. Lett. **B351** (1995) 357–368, arXiv:hep-ph/9411423 [hep-ph].

[45] Muon g-2, F. Gray, *Muon g-2 Experiment at Fermilab*, in *12th Conference on the Intersections of Particle and Nuclear Physics (CIPANP 2015) Vail, Colorado, USA, May 19-24, 2015*. 2015. arXiv:1510.00346 [physics.ins-det]. https://inspirehep.net/record/1395618/files/arXiv:1510.00346.pdf.

[46] N. Saito, J-PARC g-'2/EDM, *A novel precision measurement of muon g-2 and EDM at J-PARC*, AIP Conf. Proc. **1467** (2012) 45–56.

[47] G. W. Bennett et al., Muon g-2, *Final Report of the Muon E821 Anomalous Magnetic Moment Measurement at BNL*, Phys. Rev.

D73 (2006) 072003, arXiv:hep-ex/0602035 [hep-ex].

[48] D. Nomura, *Hadronic Contributions to $(g-2)_\mu$ and $\alpha_{\rm QED}(M_Z^2)$*, Acta Phys. Polon. **B46** (2015) no. 11, 2251.

[49] F. Jegerlehner, *Leading-order hadronic contribution to the electron and muon g-2*, EPJ Web Conf. **118** (2016) 01016, arXiv:1511.04473 [hep-ph].

[50] J. P. Lees et al., BaBar, *Precise Measurement of the $e^+e^- \to \pi^+\pi^-(\gamma)$ Cross Section with the Initial-State Radiation Method at BABAR*, Phys. Rev. **D86** (2012) 032013, arXiv:1205.2228 [hep-ex].

[51] M. Ablikim et al., BESIII, *Measurement of the $e^+e^? \to \pi^+\pi^?$ cross section between 600 and 900 MeV using initial state radiation*, Phys. Lett. **B753** (2016) 629–638, arXiv:1507.08188 [hep-ex].

[52] D. Babusci et al., KLOE, *Precision measurement of $\sigma(e^+e^- \to \pi^+\pi^-\gamma)/\sigma(e^+e^- \to \mu^+\mu^-\gamma)$ and determination of the $\pi^+\pi^-$ contribution to the muon anomaly with the KLOE detector*, Phys. Lett. **B720** (2013) 336–343, arXiv:1212.4524 [hep-ex].

[53] F. Ambrosino et al., KLOE, *Measurement of $\sigma(e^+e^- \to \pi^+\pi^-)$ from threshold to 0.85 GeV^2 using Initial State Radiation with the KLOE detector*, Phys. Lett. **B700** (2011) 102–110, arXiv:1006.5313 [hep-ex].

[54] F. Ambrosino et al., KLOE, *Measurement of $\sigma(e^+e^- \to \pi^+\pi^-\gamma(\gamma)$ and the dipion contribution to the muon anomaly with the KLOE detector*, Phys. Lett. **B670** (2009) 285–291, arXiv:0809.3950 [hep-ex].

[55] R. R. Akhmetshin et al., CMD-2, *High-statistics measurement of the pion form factor in the rho-meson energy range with the CMD-2 detector*, Phys. Lett. **B648** (2007) 28–38, arXiv:hep-ex/0610021 [hep-ex].

[56] M. N. Achasov et al., *Update of the e+ e- —¿ pi+ pi- cross-section measured by SND detector in the energy region 400-MeV ¡ s**(1/2) ¡ file1000-MeV*, J. Exp. Theor. Phys. **103** (2006) 380–384, arXiv:hep-ex/0605013 [hep-ex]. [Zh. Eksp. Teor. Fiz.130,437(2006)].

[57] H. Czyz, A. Grzelinska, J. H. Kuhn, and G. Rodrigo, *The Radiative return at phi and B factories: Small angle photon emission at next-to-leading order*, Eur. Phys. J. **C27** (2003) 563–575, arXiv:hep-ph/0212225 [hep-ph].

[58] F. Campanario, H. Czyz, J. Gluza, M. Gunia, T. Riemann, et al., *Complete QED NLO contributions to the reaction $e^+e^- \to \mu^+\mu^-\gamma$ and their implementation in the event generator PHOKHARA*, JHEP **1402** (2014) 114, arXiv:1312.3610 [hep-ph].

[59] B. Holdom, *Two U(1)'s and Epsilon Charge Shifts*, Phys.Lett. **B166** (1986) 196.

[60] O. Adriani et al., PAMELA Collaboration, *An anomalous positron abundance in cosmic rays with energies 1.5-100 GeV*, Nature **458** (2009) 607–609, arXiv:0810.4995 [astro-ph].

[61] M. Ackermann et al., Fermi LAT Collaboration, *Measurement of separate cosmic-ray electron and positron spectra with the Fermi Large Area Telescope*, Phys.Rev.Lett. **108** (2012) 011103, arXiv:1109.0521 [astro-ph.HE].

[62] L. Accardo et al., AMS Collaboration, *High Statistics Measurement of the Positron Fraction in Primary Cosmic Rays of 0.5500 GeV with the Alpha Magnetic Spectrometer on the International Space Station*, Phys.Rev.Lett. **113** (2014) 121101.

[63] R. Essig, P. Schuster, and N. Toro, *Probing Dark Forces and Light Hidden Sectors at Low-Energy e+e- Colliders*, Phys.Rev. **D80** (2009) 015003, arXiv:0903.3941 [hep-ph].

[64] J. Lees et al., BaBar Collaboration, *Search for a dark photon in e^+e^- collisions at BABAR*, arXiv:1406.2980 [hep-ex].

[65] B. Aubert et al., BaBar Collaboration, *Search for Invisible Decays of a Light Scalar in Radiative Transitions $\Upsilon(3S) \to \gamma A^0$*, arXiv:0808.0017 [hep-ex].

[66] J. Alwall, R. Frederix, S. Frixione, V. Hirschi, F. Maltoni, O. Mattelaer, H. S. Shao, T. Stelzer, P. Torrielli, and M. Zaro, *The automated computation of tree-level and next-to-leading order differential cross sections, and their matching to parton shower simulations*, J. High Energy Phys. **07** (May, 2014) 079. 158 p. https://cds.cern.ch/record/1699128. Comments: 158 pages, 27 figures; a few references have been added.

[67] R. Essig, R. Harnik, J. Kaplan, and N. Toro, *Discovering New Light States at Neutrino Experiments*, Phys.Rev. **D82** (2010) 113008, arXiv:1008.0636 [hep-ph].

[68] S. Jadach, W. Placzek, and B. F. L. Ward, *BHWIDE 1.00: O(alpha) YFS exponentiated Monte Carlo for Bhabha scattering at wide angles for LEP-1 / SLC and LEP-2*, Phys. Lett. **B390** (1997) 298–308, arXiv:hep-ph/9608412 [hep-ph].

[69] D. Karlen, *Radiative Bhabha Scattering for Singly Tagged and Untagged Configurations*, Nucl. Phys. **B289** (1987) 23–35.